Quantification of Three-Dimensional Left Ventricular Segmental Wall Motion and Volumes from Gated Tomographic Radionuclide Ventriculograms

Tracy L. Faber, Ernest M. Stokely, Gordon H. Templeton, Marvin S. Akers, Robert W. Parkey, and James R. Corbett

Radiology Imaging Center, University of Texas Southwestern Medical Center at Dallas, Dallas, Texas

Tomographic radionuclide ventriculograms may be used for three-dimensional wall motion analysis. We propose that automatic quantification of these images is possible, and here we describe the implementation and validation of a method to perform this task. Automatic computer methods were developed to locate the left ventricular (LV) endocardial surfaces in all time frames of the cardiac cycle. Global, regional, and local motion and volume were computed. Results were displayed using three-dimensional graphics. The methods were validated using phantom, canine, and human studies. Actual phantom values correlated well with experimentally determined volumes, $y = 1.01x + 1.29$ml, $r = 0.99$. In the canine model, the LV endocardial surfaces were located to within an average of 1.9 mm and 3.7 mm at end-diastole and end-systole, respectively. Areas of obvious wall motion abnormalities in automatically processed patient studies corresponded well with angiographically documented coronary artery disease. End-diastolic and end-systolic volumes computed automatically from single photon emission computed tomography averaged errors of 9% and 38%, respectively, when compared with contrast ventriculographic volumes. These results indicate that it is possible to automatically identify the left ventricular endocardial surface in gated tomographic radionuclide ventriculograms. The location of these surfaces corresponds well with the location of implanted endocardial markers, and global volume computed from these surfaces corresponds well with known volumes.

J Nucl Med 30:638–649, 1989

Gated tomography is a relatively new advance in cardiac imaging with single photon emission computed tomography (SPECT). It allows the visualization of the four-dimensional distribution (three cartesian coordinates and time) of the radionuclide within the heart. In the case of tomographic radionuclide ventriculography (TRVG) the motion of the endocardial boundary of the radiolabeled blood pool can be determined. A representative TRVG image can be seen in Figure 1.

Planar radionuclide ventriculography (RVG) has been shown to be useful in analyzing regional left ventricular (LV) function, specifically, segmental wall motion, regional ejection fraction, and phase analysis (*1–7*). However, planar RVG suffers from the same problems as all imaging modalities using projection images. They are two-dimensional compressions of three-dimensional data, and important structures in such images may be hidden or masked by objects in front of or behind them. True volume or area calculations cannot be performed; although relative volume may be estimated from count statistics (*8–10*), any absolute volume determination must be based on some assumption regarding the three-dimensional geometry of the LV (*11–13*).

Tomographic imaging largely solves these problems for RVGs by separating the right and left ventricles in space and thus allowing true three-dimensional volume calculations to be performed (*14–16*). TRVG has been used in a number of studies for the analysis of wall

Received Feb. 19, 1988; revision accepted Jan. 5, 1989.

For reprints contact: Tracy L. Faber, PhD, Radiology Imaging Center, University of Texas Southwestern Medical Center at Dallas, 5323 Harry Hines Blvd., Dallas, TX 75235-9058.

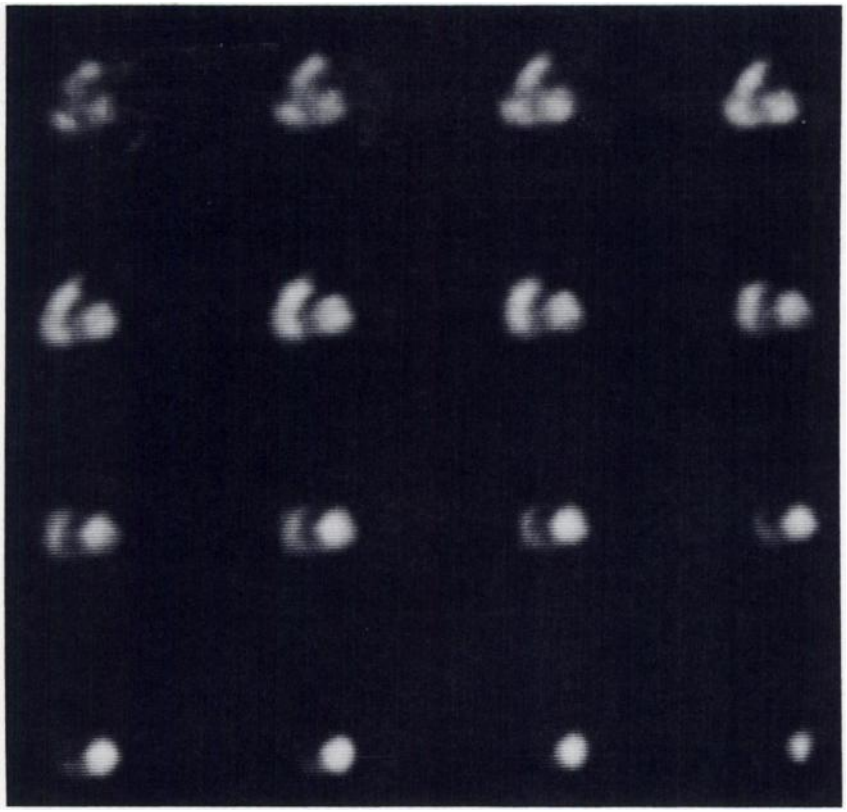

FIGURE 1
Representative tomographic radionuclide ventriculogram. These are short axis slices at end-diastole.

motion in the third dimension (*16–18*) and appears to offer a significant advance over planar imaging for this purpose. In the previous studies from this laboratory, TRVG was found to have a greater sensitivity and specificity for the detection of wall motion abnormalities than either RVG or cineangiography (*16*).

If TRVG is to be used for quantitative analysis of LV wall motion, automatic processing methods and three-dimensional display capabilities are needed. Because tomographic imaging dramatically increases the volume of data as compared to planar imaging, manual processing is usually too labor intensive and time-consuming to be practical. Automatic computer methods reduce time and effort, and should give more reproducible results.

Unfortunately, three dimensional quantification of TRVG is extremely complicated. Automatic edge detection, boundary tracking, and wall motion analysis and display are more complicated in three dimensions and have not been investigated as thoroughly as two dimensional methods. In previous studies by other investigators, only selected tomographic slices have been analyzed using two-dimensional processing techniques; i.e., no true three-dimensional analysis methods have yet been implemented for TRVG. Methods for quantifying information in three-dimensional slices of TRVG images are similar to those for RVG. Automatic edge detection methods are usually based on either thresholding or local gradient operators (*15,19–21*). Boundary tracking techniques for two-dimensional wall motion analysis utilize models of LV contraction. These models usually assume that LV motion is either radial towards some centroid, perpendicular to the long axis, or perpendicular to a tangent to the boundary (*22–32*). Many different parameters of or related to LV volumes and function can be calculated once the LV boundaries have been determined (*2–6*).

We approach the problem using a completely three-dimensional approach. We have designed and validated computer algorithms that automatically perform almost all of the needed steps for determining regional LV wall motion from TRVG while utilizing all the available four-dimensional data. This system uses thresholding for edge detection and bijective mapping for endocardial boundary tracking. It calculates local, regional, and global volume and motion, and displays the results using three-dimensional graphics.

The methods' accuracy was measured using phantom and in vivo studies. Edge detection was validated globally using phantom studies. A local measure of edge detection accuracy was obtained by using radioactive markers implanted next to the endocardial surface of the LV in canines. This marker system is unique, but analogous nonradioactive marker systems have been used previously to investigate normal heart motion (*33, 34*) and to validate methods of regional wall motion quantification in two-dimensional with contrast ventriculography (*28–30*).

Finally, patient studies were processed with this system. The results of the automatic processing were compared to the known distribution of coronary artery disease. These patient studies demonstrate the projected clinical usefulness of this system.

METHODS

Study Protocols

Phantom studies. The only methods available for measuring LV volumes in vivo are highly invasive and imprecise. Therefore, a phantom study was performed to validate the system's accuracy in global volume calculations. Pear-shaped boiling flasks of four different nominal volumes—25, 50, 100, and 125 ml—were used. They were filled with technetium-99m (^{99m}Tc) solution of 1 mCi/50 ml and suspended in the center of a 18-cm-diameter cylinder filled with water. The flasks were not suspended in any standard orientation. Projection images were obtained over 360° circular orbits at 120 angles and recorded as 64^2 matrices. Acquisitions required ~20 min and resulted in average counts of 5.0×10^5 counts/study. Actual flask volumes were measured using a graduated cylinder. Reconstructions were performed by filtered backprojection; the filter used was a Butterworth with a cut-off frequency of 0.4 pixel and an order of 4. Reconstructions were processed in the same manner as described in the following section, with the exception that each flask was analyzed as though it were the first frame of a gated study, i.e., no time constraints were employed.

Because the thresholds used in edge detection are selected by the user, it is imperative that they be chosen accurately. Edge detection and volume calculations were repeated at the chosen level ± 8 Gray levels, in order to investigate the effect of variations in the chosen threshold.

Animal studies. Animal experiments were performed in order to validate the methods in vivo. Ideally, boundary detection could be validated locally by comparing the locations of all 288 identified endocardial surface points to the actual positions of those points on the endocardium. Unfortunately, there is no way to validate all of the actual endocardial points that correspond with those indentified; realistically, only a few points could be marked in such a way as to be unequivocably identified by SPECT or any imaging modality. Six gadolinium-153 (^{153}Gd) point sources (0.5 mCi each) (Dupont Company, No. Billerica, MA), were used as radioactive endocardial surface markers (*33*). The sources were encased in cylindrical epoxy 2 mm high and 2 mm in diameter. Five mongrel dogs were anesthetized using i.v. nembutal, 25 mg/kg, and underwent left thoracotomy. Each source was implanted near the endocardium of the LV using the technique of Mitchell et al. (*33*). Sources were placed at the apex and at the first bifurcation of the left main coronary artery. Four additional sources were placed in the anterior, posterior, septal, and lateral walls in a plane perpendicular to and bisecting the left ventricular long axis. Each dog was allowed to recover for 1 wk prior to study.

Each dog was again anesthetized using i.v. nembutal, 25 mg/kg. Single photon tomographic imaging was performed using a rotating Anger camera (Omega 500S, Technicare, Solon, OH). Energy discrimination was provided by 10% windows centered on the 100 keV and 140 keV photopeaks of ^{153}Gd and ^{99m}Tc, respectively. While imaging of the ^{153}Gd endocardial markers was being performed, the animals' red blood cells were labeled in vitro with 0.43 mCi/kg of ^{99m}Tc (*35*). The animals were positioned supine and were not moved between image acquisitions. Cardiac output (CO) measurements were obtained both prior and following each tomographic acquisition using a thermodilution catheter placed in the pulmonary artery.

For each acquisition, gated projection images were collected at 3° intervals over 180° from right lateral to left lateral, 16 frames per cardiac cycle at each projection. Images were acquired at a digital resolution of 64^2, and with the hardware zoom used for the animal studies the final pixel dimension was 0.387 cm × 0.387 cm. Both acquisitions required ~35 min. The TRVG study contained ~4.0×10^6 cts/frame. One-pixel-thick transaxial sections were reconstructed by filtered backprojection using a Butterworth filter of cutoff = 0.4 pixel and order = 4. Short-axis sections were extracted from the reconstructed volume so that the LV long axis was oriented vertically, the standard orientation for this investigation. Both the TRVG studies and the gated ^{153}Gd marker studies were reconstructed using exactly the same parameters, so that the images could be corresponded pixel-for-pixel.

The TRVGs were processed using the analysis methods discussed in the next section with no modification for canine as opposed to human studies. The ^{153}Gd marker locations were determined from the reconstructed gated marker images. The most intense pixel in the region of each marker was considered to be the location of the marker. The radioactive markers were carefully dissected from the myocardium following death of the animals. The distance of each marker from the endocardial surface was measured for the final three dogs; this distance was called the bias distance.

In order to determine the accuracy of regional edge detection, a given marker in the gated marker image was corresponded to the closest experimental surface point in the TRVG image. The distance, r^*, of the closest identified point from the center of the LV long axis was computed using the TRVG image. The distance of the marker from the center of the long axis was calculated using the gated marker image and the bias distance was subtracted to give r, the distance of the actual endocardial surface point from the center of the long axis. The difference between r and r^* was considered the error in edge detection (Fig. 2).

Global surface detection was validated first by comparing actual with experimental stroke volume (SV). Actual SVs were determined by averaging the SVs determined from thermodilution COs and HR measurements obtained before and after TRVG acquisition. Experimental SVs were those determined from the TRVGs.

Patient studies. Four patients with angiographically documented coronary artery disease (CAD) were studied. Contrast ventriculography and TRVG were performed on all patients. Ventricular volumes at ED and ES were measured using the geometric method of Greene et al. (*11*) as modified by Kennedy et al. (*13*). Tomographic imaging was performed within 14 days of catheterization, and there were no changes in medication or patient condition between studies.

TRVGs were performed on four patients. Red blood cells were labeled using the methods described in (*35*); the typical

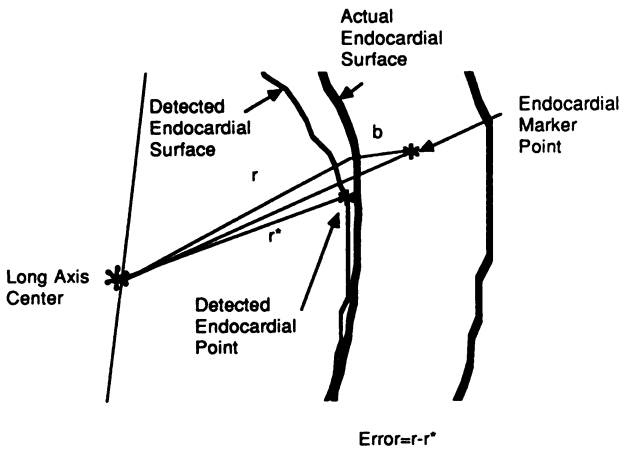

FIGURE 2
Diagram of geometry used to compute edge detection error.

radioactive dose was 0.43 mCi/kg. For three patients, the rotating gamma camera was the GE400T (GE, Milwaukee, WI), and for one patient the camera was an Omega 500S (Technicare, Solon, OH). Energy discrimination was provided by a 15% window centered on the 140-keV photopeak of ^{99m}Tc. The patients were positioned supine, and gated projection images were collected at 6° intervals over 180° from right anterior oblique to left posterior oblique, 16 frames per projection. Images were acquired at a digital resolution of 64^2, and with the hardware zooms used the final pixel dimensions were 0.625 cm × 0.625 cm for the 400T camera and 0.58 cm × 0.58 cm for the Omega 500S. Acquisitions typically required 30–35 min and the resulting frames contained ~2.5×10^6 cts/frame. Transaxial sections 1 pixel thick were reconstructed by filtered backprojection with a Butterworth filter of cutoff = 0.4 pixel and order = 4. Short axis sections were extracted from the reconstructed volumes so that the LV long axis was oriented vertically.

Reconstructed sectional images were processed as described in the following sections. Total LV volumes at ED and ES were calculated and compared to the cineangiographic values. Local motion and volume changes from ED to ES were calculated and color-coded onto the LV wire frame surface of each patient. The areas of reduced motion were compared with the known distribution of coronary artery stenoses (>70% luminal diameter narrowing).

Analysis Methods

Edge detection. The edge detection algorithm was designed to require the least possible operator interaction. The aortic valve plane and the initial surface detection thresholds for the apex and base of the LV at end-diastole (ED) and end-systole (ES) required operator input. The system is otherwise entirely automatic. Initially, the four-dimensional images f(x,y,z,t) supplied to the system were assumed to be oriented so that the LV long axis was parallel to one of the image coordinate axes, specifically, the z-axis. Contiguous horizontal long axis sections were displayed for both the ED and ES time frames. The operator determined the center of the aortic valve plane and the apical point for both ED and ES images. The apical point was chosen by the operator in these frames simply to give an initial estimate of the location of the center of the LV long axis, xcen,ycen,zcen; it was subsequently recalculated automatically for the ED and ES frames as well as for all other frames. The location of the valve plane center was determined at all other frames by assuming that it moved linearly between its operator-chosen positions at ED and ES.

Thresholding was used to determine endocardial surfaces. Manually set thresholds at end-diastole and end-systole were used to predict thresholds for all frames. Horizontal long axis sections of the tomographic studies were displayed and the results of choosing different threshold values were seen interactively by the user. Two thresholds were determined for each frame, one for the apical ¾ of the LV and another for the valve plane region. This was necessary because a slightly higher threshold was needed to distinguish the left atrium from the left ventricle than was needed to distinguish the right ventricle from the left ventricle. Both apical and valve plane thresholds were assumed to vary linearly between ED and ES. Within each frame, thresholds varied linearly along the direction of the long axis (the z-axis) between the apical and valve plane thresholds, starting ¾ of the way from the apex to the valve plane. This is illustrated in Figure 3.

Following thresholding, endocardial surfaces were determined for all frames. First, the apical point was identified automatically. The automatic method basically consisted of finding the most inferior point within a set distance from the LV center but still above the edge detection threshold. It has been shown previously that this method is quite accurate for finding the apical point when the LV is oriented so that the long axis is perpendicular to the z axis (*36*).

Edge points were determined in spherical coordinates, with the origin being the midpoint of the long axis of the LV calculated for each time frame. In this coordinate system, the images were described as $f(\rho, \theta, \phi, t)$. The surface was described as the set of radii ρ, which are a function of (θ, ϕ, t). At any given pair of angles (θ, ϕ), at any given time frame (t), the

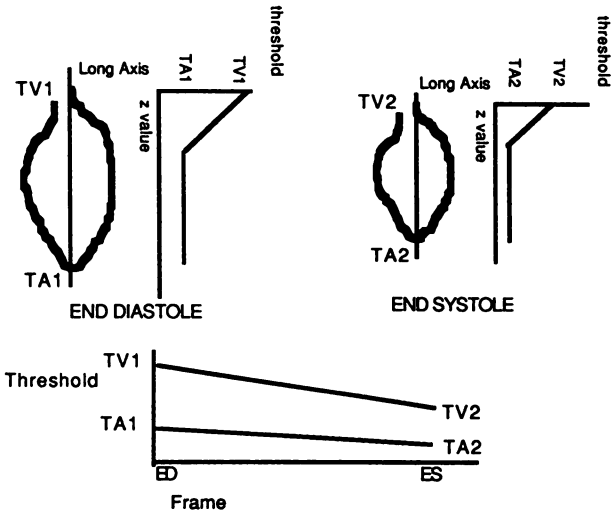

FIGURE 3
Diagram of variable thresholding method. TV1 and TV2 indicate the user-set thresholds for the valve plane region at end-diastole and end-systole, respectively. TA1 and TA2 indicate thresholds for the apical region at ED and ES, respectively.

surface point was considered to be that point at maximal distance from the origin, but still above the threshold for the z-coordinate of that point. Linear interpolation of image intensity was performed in order to determine the radius to within ±0.1 pixel. Several heuristics were introduced into the edge finding process; the surface was constrained to be smooth, continuous, and convex. Wall motion was also constrained to be smooth and continuous. If an edge point $\rho(\theta_i, \phi_j, t_k)$ did not meet the constraints, predictions about the radius at θ_i, ϕ_j, t_k were made. These predictions used adjacent values of ρ and previous surface motion, i.e.,

$$\rho(\theta_i, \phi_j, t_k) = 1/4(\rho(\theta_i, \phi_{j-1}, t_k)) + 1/4(\rho(\theta_{i-1}, \phi_j, t_k)) + \rho(\theta_i, \phi_j, t_{k-1}) - 1/2(\rho(\theta_i, \phi_j, t_{k-2})).$$

Edge tracking. Tracking of edge points from frame to frame was accomplished by a three-dimensional extension of the bijective mapping method described by Doss et al. (*27*). This technique tracks points associated with features that can be reliably located in every frame and uses the motion of these points to predict the motion of additional points. This method has the unique ability to improve as the data improves and more points can be tracked accurately. For TRVG, the two points that could be tracked most accurately were the aortic valve plane and the apex. The valve plane was determined manually at ED and ES and assumed to move linearly between these two time frames. The apex was determined automatically at each time frame as described in the previous section. The following implementation of a bijective mapping technique was used to track the rest of the surface points.

The LV was considered to be a globe with the valve plane and apex at the north and south poles, respectively. The total length of the equator of the LV was calculated by identifying 120 points on this latitude line using the edge detection methods described in the previous section. The lengths of the line segments connecting the points were added together, and the total length of the equator was divided into 24 segments of equal length. The middle of the lateral wall was the starting point ($\theta = 90°$, $\phi = 90°$). Note, the left ventricle was assumed not to rotate about its long axis during contraction. The 24 equatorial points then define the angular locations of 24 longitude lines. Sixty points along each longitude line were identified so that the length of each could be calculated. Six equally spaced points between each pole and the equator were then computed. Thus, a total of 288 LV surface points were found for each time frame.

Analysis. The points on the longitude and latitude lines were connected into a standard set of triangles, thus creating a polygonal approximation to the LV. Area, volume, and motion measurements were based on this polygon. Because the vertices of the triangles are tracked points, a correspondence between the triangles themselves can be assumed, and local changes in surface area with time can be calculated. If the midpoint of the long axis is added as a central point, tetrahedrons consisting of this point plus the surface triangles are defined. The volume of any tetrahedron (see Fig. 4) can be defined as $1/12(\vec{p}_1 \times \vec{p}_2 \cdot \vec{p}_3)$, where $\vec{p}_1$ and $\vec{p}_2$ are vectors from one of the triangle vertices, p, to the remaining vertices p_1 and p_2, and $\vec{p}_3$ is the vector from p to the center point p_3. The operations are cross and dot products, respectively. Therefore, local volumes and their changes with time throughout the cardiac cycle can be computed. Also, the heights of these tetrahedrons and their changes with time can be used as measures of the motion of LV surface points in the radial direction.

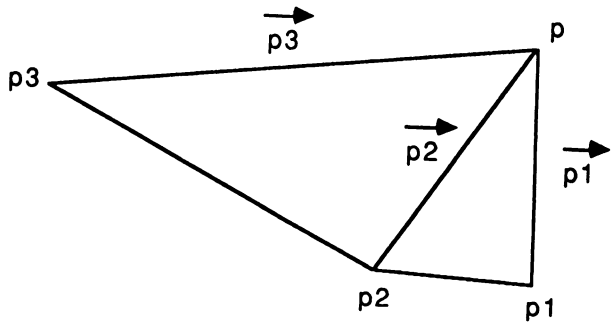

FIGURE 4
Geometry of tetrahedron.

Regional measures of area, volume, and motion were made by dividing the surface of the LV into nine regions based on latitudinal and longitudinal positions: apex, anterior, superior, lateral, basal-lateral, septal, basal-septal, inferior, and posterior. The total surface area, volume, and average height for these regions were calculated for each frame and graphed versus time. These areas and volumes were summed for the entire polygonal LV, and actual measures of global LV area and volume were obtained for each time frame.

Display. The triangulated LV surfaces were displayed with three-dimensional graphics using representations called "wire frames", which depict surfaces as skeletons rather than as solids (*37*). These wire frame representations were generated for all time frames of the cardiac cycle. The display software also allowed the wire frame to be rotated about any of the three coordinate axes, scaled, and saved as an image.

In addition to a global display of the LV, volume and area changes and motion were color-coded onto the LV surface. The change in area of each triangle and the change in volume or height of each tetrahedron were computed between ED and ES. These differences were scaled so that relatively large changes (LV average + s.d.) were displayed as pink-white, and relatively small changes (LV average − s.d.) were displayed as blue-violet. Average changes were displayed as green. The wire frames were also depth shaded to add three-dimensional depth cues to the display.

Regional areas, volumes, and motion were also displayed as curves versus time. The LV wire frames and curves were color-coded as to anatomical region so that the positions of these regions and the corresponding curve data could be readily visualized.

RESULTS

Phantom Studies

The volumes determined experimentally from the reconstructed transaxial slices of the pear-shaped flasks were quite similar to their actual volumes (Fig. 5). Note that the actual flask volumes of 32, 60, 109, and 164 ml were larger than the nominal volumes of 25, 50, 100, and 125 ml. The correlation of the experimental

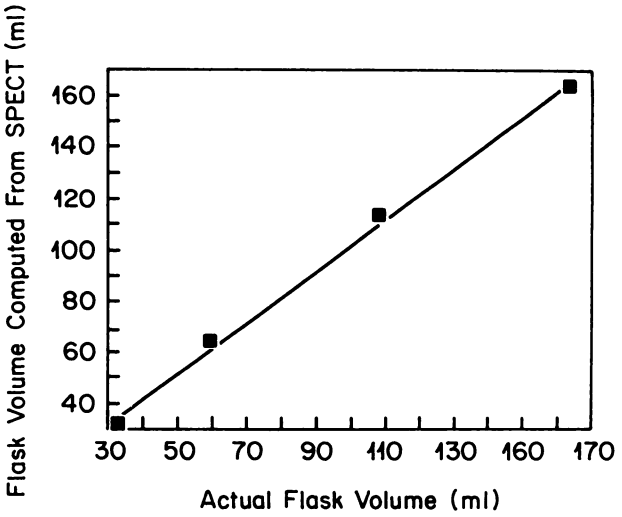

FIGURE 5
Results of volume comparison in phantom study.

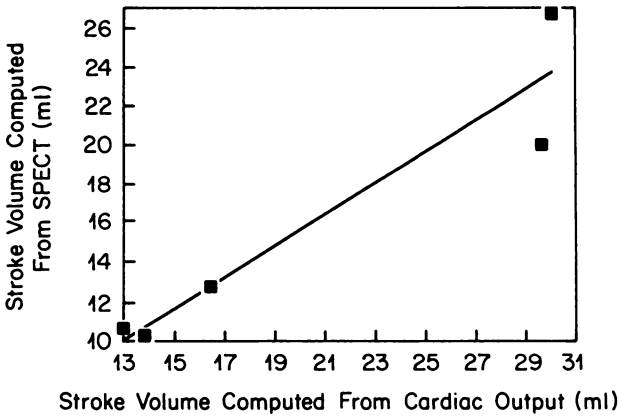

FIGURE 7
Results of stroke volume comparison in animal study.

flask volumes (V_{exp}) with actual flask volumes (V_{ac}) was very close: regression equation $V_{est} = 1.01\ V_{ac} + 1.29$ ml, r = 0.999, where V_{est} is estimated volume. The standard error of the y estimate (s.e.e.) was 2.94 ml.

Variations in threshold about the user-set value had a linear effect on experimental volume (Fig. 6). The slopes of the lines relating threshold to volume were −0.56 ml/G level, −.95 ml/G, −1.11 ml/G, −1.99 ml/G for the 25-, 50-, 100-, and 125-ml flasks, respectively. When thresholds are chosen inaccurately, the volume changes vs. threshold (i.e., slopes), normalized for total flask volumes, provide a measure of error when thresholds are chosen inaccurately. These errors were 1.8%/G, 1.6%/G, 1.0%/G, and 1.2%/G for the smallest to largest flasks, respectively.

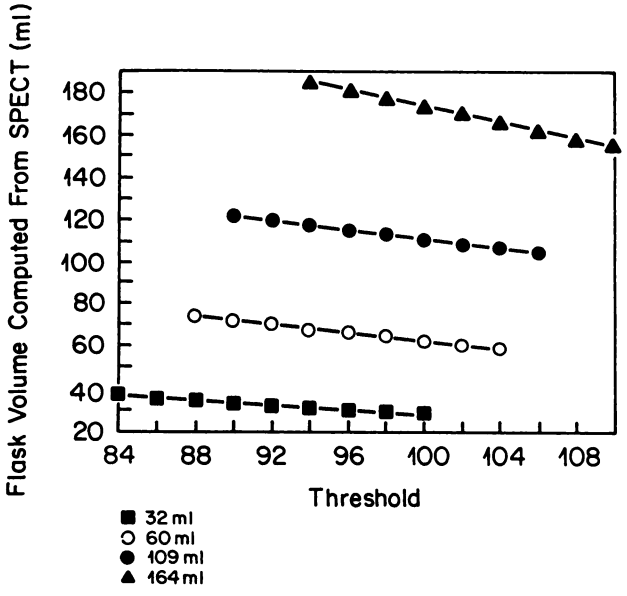

FIGURE 6
Results of varying user-set threshold in phantom study.

Animal Studies

Experimental stroke volumes (SV) correlated well with thermodilution SV; however, the experimental values averaged only 78% of the thermodilution (Fig. 7). The regression equation was $SV_{es} = 0.79\ (SV_{exp}) - 0.24$ ml, r = 0.997, s.e.e. = 2.68 ml, where SV_{es} is estimated stroke volume and SV_{exp} is experimental stroke volume.

The absolute distances of the experimental surface points from the actual endocardial surface at ED were quite small in most cases. The average of the absolute values of these distances was 1.9 mm, only 0.5 pixel. In general, ES errors are larger. The distances of the experimental points from endocardium at each of the six marker locations are listed in Table 1. Note, a negative distance indicates that the surface point was found outside of the endocardial surface.

Patient Studies

Comparisons between ED and ES volumes computed by CVG and TRVG are shown in Table 2. Local motion or volume changes from ED to ES, color-coded onto the LV endocardial surface at ES of the four patient studies are shown in Figure 8. The first three patients (Fig. 8A–8C) had 90% or greater LAD stenoses; the fourth patient (Fig. 8D) had a 99% right coronary artery stenosis and a 50% circumflex coronary artery stenosis. Once again, purple or violet regions are those which exhibited reduced local motion or volume changes. The correlation of quantified motion to the known condition of this small number of patients was obviously quite good.

A cyclic display of the three-dimensional wire frame LV endocardial surface for the patient in Figure 8B is shown in Figure 9. This patient had a 90% LAD stenosis. The abnormal shape and movement of the apical and lateral regions of the LV are clearly demonstrated.

TABLE 1
Distances of Experimental Surface Points from Endocardial Surface for Animal Studies

	Dog 3		Dog 4		Dog 5	
	ED	ES	ED	ES	ED	ES
Apical point	−4.9*	11.7	−3.0	−0.2	1.4	3.7
Basal point	0.1	4.7	1.6	3.3	−1.1	2.7
Septal point	0.4	2.1	0.2	−0.6	−1.3	−0.2
Lateral point	4.9	7.1	4.0	6.5	−0.2	−0.8
Posterior point	3.2	4.7	−1.1	0.1	1.7	3.4
Anterior point	−1.4	6.8	−2.5	−0.3	1.8	6.8

* All distances in mm. Negative distances indicate that the experimental surface point was found outside the endocardial surface.

Time-volume curves for the nine regions of the LV of the patient in Figure 8A are shown in Figure 10. Here, the time course of regional volume changes indicated abnormally reduced motion of the apical and septal regions. The color-coded wire frame allows the user to visualize the extent of the regional abnormalities.

DISCUSSION

Tomographic RVGs require more acquisition time than planar RVGs. Acquisitions take 30–35 min; this is twice as long as a typical ungated tomographic study. This acquisition time is not prohibitive, but it is does preclude exercise studies. However, newer gamma cameras with multiple heads can divide acquisition times in half or even one-third; such advances may make stress tRVG practical.

Processing time is longer with gated tomographic studies than with gated planar studies. Tomographic reconstructions must be performed and oblique slices are often required. With our system, these two steps take 45 min. The additional quantitative processing described in this manuscript then requires another 20 min. Note that the largest amount of processing time is in reconstruction and oblique slice creation; one reason is that the computer used for these steps was a Technicare 560 computer which was built in the early 1980s. With improved technology, the speed of these operations could be increased. Also note these processing steps are not user-intensive and could theoretically be run in a background-type environment while other primary tasks such as additional acquisitions are running. These facts suggest that gated tomography is already realistic and will become even more so.

TABLE 2
Comparisons of End-diastolic and End-systolic Volumes Computed from Contrast Ventriculograms and Tomographic Radionuclide Ventriculograms

Patient no.	End-diastolic		End-systolic	
	CVG	Tomo	CVG	Tomo
1	126*	120	63	33
2	101	117	62	45
3	126	137	52	52
4	138	130	34	47

* All volumes in ml.

This study has demonstrated that it is possible to automatically determine left ventricular endocardial surface boundaries in tomographic radionuclide ventriculograms. It has shown that global volume measurements and regional surface detection may be accurately performed with minimal operator input. The color-coded three-dimensional wire frame displays of the detected LV surface give a clear and understandable anatomically and physiologically important presentation of the data.

Thresholding is a simple technique easily applied to medical images. Chow and Kaneko (*38*) found, as we did, that one threshold is not sufficient for delimiting the LV in RVG. They developed a variable thresholding technique according to local histograms. Tauxe, et al. (*39*) used a statistical threshold to accurately determine phantom volumes using SPECT. Although manually set thresholds are less reproducible, the results of this study indicate that reasonable accuracy of surface detection is possible with manually set thresholds.

There is no existing three-dimensional model of myocardial contraction that can be used to track the endocardial surface. In two dimensions, it is often assumed that all points contract radially toward some common center, but this is a simplifying assumption that has been shown to be inaccurate (*30–32*). One two-dimensional method tracks as many points as possible and interpolates between tracked points to predict the motion of additional surface points (*29*). Good correlation between endocardial markers and motion derived from contrast ventriculograms has been demonstrated with this model. Although the algorithm developed for this study does not track a large number of points, as instrumentation improves and anatomical features become more distinct in the scans, the tracking can be improved accordingly.

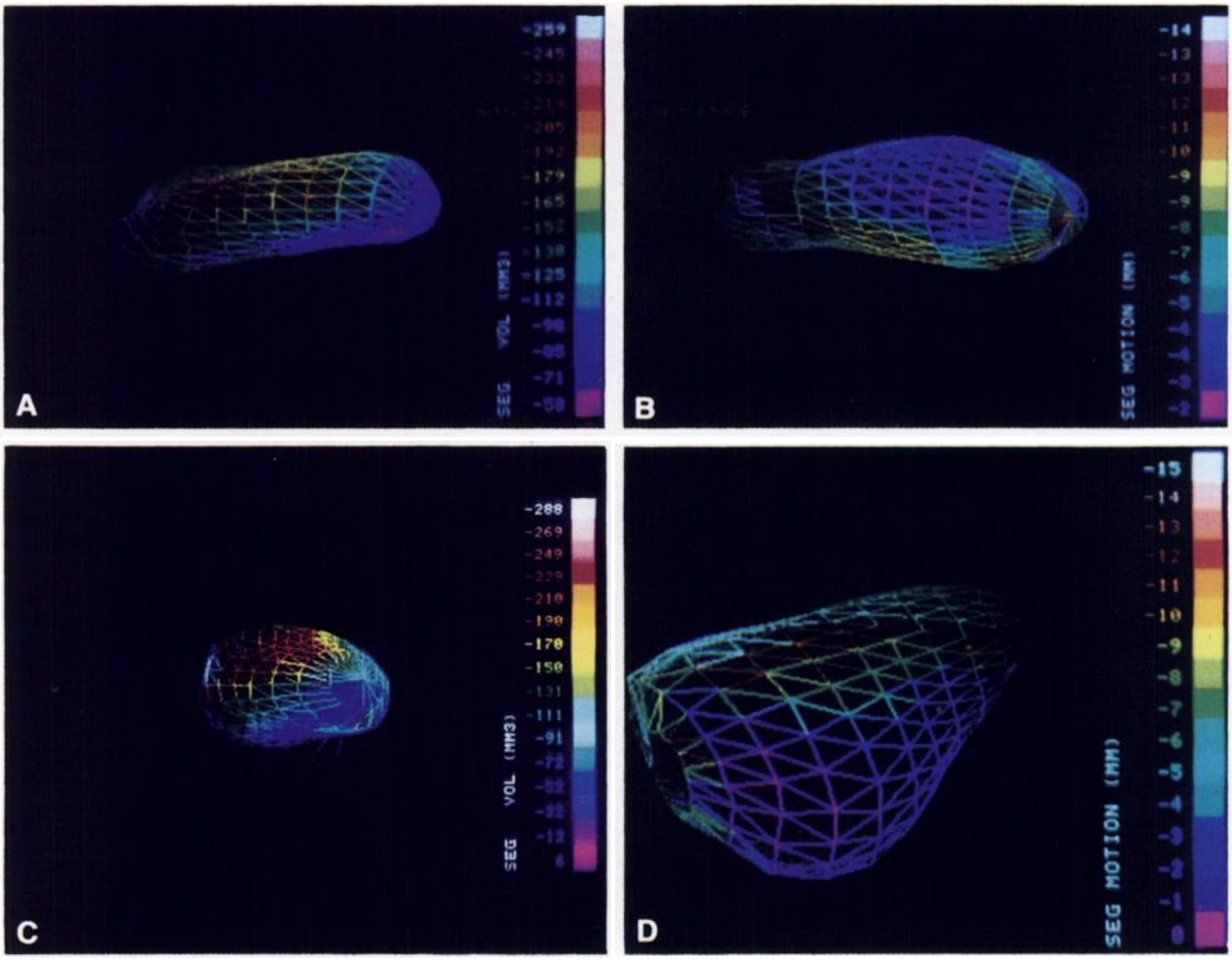

FIGURE 8
Color-coded wire frame representations of the left ventricles of four different patients. A: Reoriented LAO view of LV with a 100% left anterior descending coronary artery (LAD) stenosis. B: Reoriented LAO view of LV with a 90% right coronary (RC) and 90% LAD stenosis. C: LAO view of LV with a 90% LAD stenosis. D: RPO view of LV with a 99% RC stenosis and 50% circumflex artery stenosis.

One weak point of our implementation is the manual selection of the aortic valve plane. The assumption that the LV does not rotate about its long axis is also incorrect; however, currently the resolution of gated blood-pool tomograms is such that the rotational motion of the LV about its long axis is quite difficult to resolve accurately.

The variables computed and displayed in this study were straightforward. Volume, area, and radial motion can be easily understood and verified. LV volume from tomograms has been computed by other investigators using two different methods. Geometric methods such as those used here rely on determining the LV surface so that the number of pixels within the LV can be counted. Volumes can be computed when the pixel dimensions are known. Count-based methods identify the LV "region" and the count rate of a "LV pixel." The total LV volume is determined by summing all pixels in the region after weighting each pixel by its count rate. Graham and Caputo (*14*) suggest that the count-based method may be the more reliable because it does not depend upon accurate edge detection, and because it takes partial volume effects into account. However, it does require a fairly accurate estimation of the "LV region," i.e., volume measurements will obviously be inaccurate if atrial and/or right ventricular pixels are included in the region. Attenuation and artifacts may also cause pixel intensity variations that would introduce inaccuracies. The geometric method was used here primarily because of the need to solve the LV surface detection problem with subpixel accuracy for quantitative wall motion analysis; therefore, this same information was readily available for volume calculations.

The phantom, canine, and human studies were used to validate the methodologies. In each case, acquisitions were performed to allow the best possible reconstructions. Since the phantom was cylindrical and uniformly

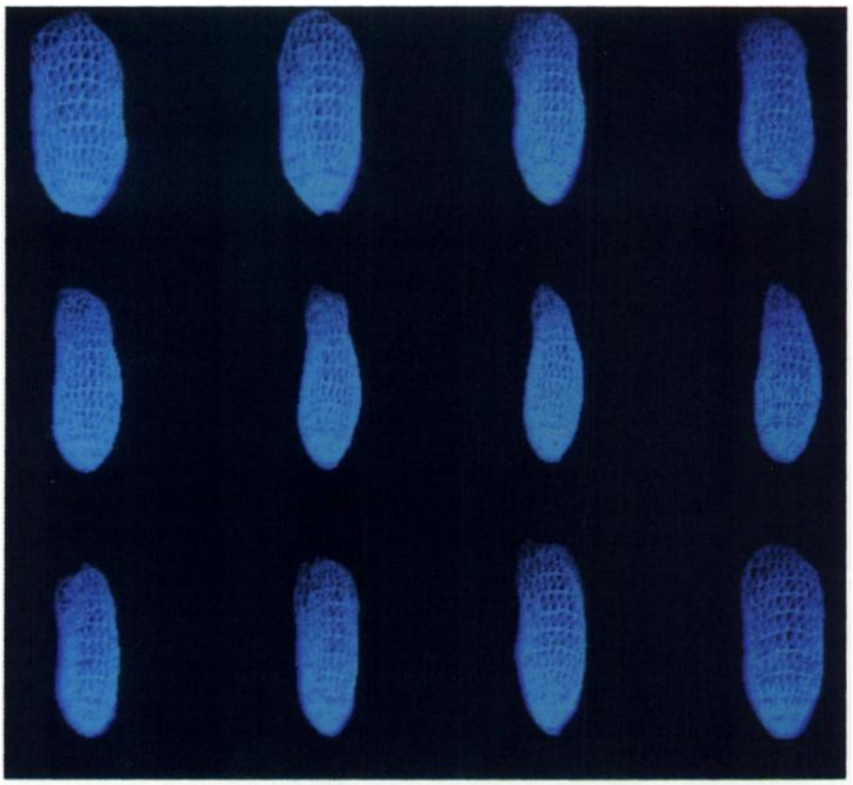

FIGURE 9
Cyclic display of the wire frame representation throughout the entire cardiac cycle; this is the same patient as in Figure 8B.

attenuating, and because the flasks were not suspended in any standard orientation, there were no severely attenuated projections that would degrade the reconstruction. For this reason, 360° acquisitions were used for the phantom studies.

For both canine and human studies, however, attenuation and time considerations indicated 180° acquisitions. By eliminating the badly attenuated posterior projections, we hoped to improve the resolution and contrast of the reconstructions. Tamaki et al. (*40*) showed that for nonattenuation corrected tomographic thallous chloride perfusion studies, 180° acquisitions gave better contrast and resolution in the reconstructions than 360° acquisitions. We did not repeat this investigation for tRVG reconstructions; however, we have found that 180° tRVG reconstructions generally demonstrate better contrast than 360° reconstructions.

Reconstructions of the cardiac blood pool are best when they are created from those projections that are closest to the left ventricle. In canines, the heart is located more anteriorly than in humans, where the heart is located to the left of center and anteriorly. For this reason, we acquired 180° projections from right lateral to left lateral in dogs, and from right anterior oblique to left posterior oblique in patients.

For both canine and patient studies, 16 time frames per beat were acquired. It has been shown that a framing rate of 20 frames/sec is sufficient for measuring ejection fraction reliably (*41*). In that study, the average heart rate of the patient population was ~72 bpm, and thus the average number of frames/cardiac cycle was 16.7. If volumes can be reliably measured at these framing rates, then it can be assumed that wall position, and therefore wall motion, can also be measured accurately.

However, these same investigators also showed that measures of peak ejection rate and peak filling rate require slightly higher framing rates. This is because computing the maximum change in volume with time requires calculation of the differential of the volume vs. time curve. The accuracy of this differential will improve as more points are added by increasing the framing rate. Thus, rates of change of volume, as well as rates of change of wall position (i.e., velocity) may require higher framing rates than 16/cardiac cycle.

The results from the phantom studies demonstrated a high degree of accuracy for measurement of volume. Errors were largest for the two smallest flasks. There are several potential explanations for this finding. Their boundaries were, in general, further away from the detector, and thus their reconstructions were more likely affected by scatter and attenuation. The smaller flasks have fewer total counts (less volume) and hence, more Poisson noise. Also, the smaller flasks have a higher surface area to volume ratio than the larger flasks; therefore, partial volume errors, i.e., thresholding errors that falsely include edge pixels as flask when they are actually background, or falsely exclude edge pixels as background when they are actually flask, should be proportionately larger for the small flasks.

As mentioned previously, the threshold decision is

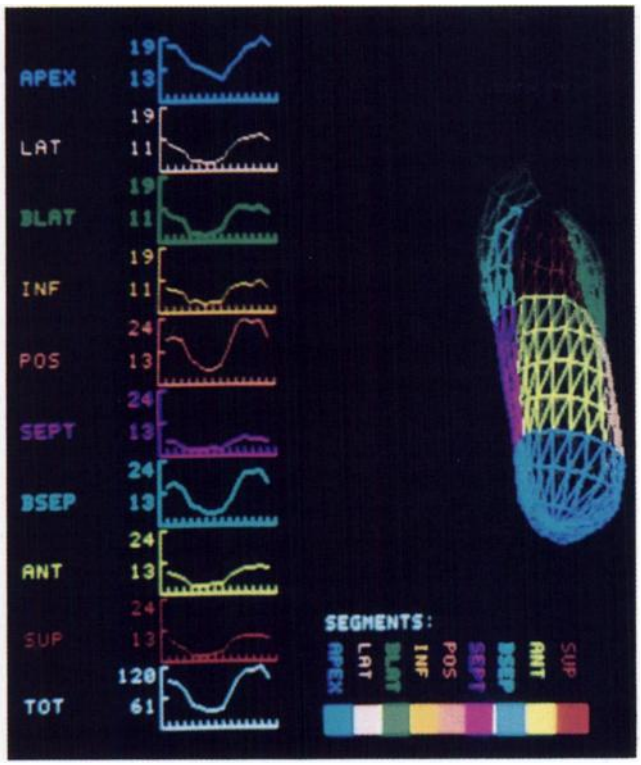

FIGURE 10
Time-volume curves and the corresponding regions of the LV which they represent; this is the same patient as in Figure 8A.

crucial to accurate volume measurements. Because there were no surrounding structures to provide a frame of reference, setting thresholds was especially difficult for the phantom studies. The presence of the ventricular and atrial septa provide the user with intuitive information of acceptability of threshold limits for the edges of the cardiac ventricles.

The animal studies also demonstrated that ventricular volume can be accurately determined using these techniques. In addition, they showed that at end-diastole at least, regional surface detection is accurate. Distance of the experimentally determined endocardial surface points from the endocardial marker locations were quite small at ED, within 5 mm in all cases. Five millimeters is only 1.4 pixel, and can be easily explained by inaccuracies in choosing the radioactive marker locations in the gated marker images and in choosing the best threshold for the tomographic blood-pool images.

Surface detection errors at end-systole were, in general, larger than those at end-diastole. This is primarily because end-systolic measurements of surface detection accuracy incorporate bias distance errors. It cannot be assumed that points deep in the myocardium several millimeters from the endocardial surface move in the same way as those on the endocardial surface, especially as much of the decrease in chamber volume during systole is accounted for by wall thickening. Other investigators have surmised that the thickening of papillary muscles and infolding of endocardial trabeculations squeeze blood out of the regions in between them and "decouple" midwall marker motion and endocardial dynamics (*30*). The extent of this bias distance error is probably impossible to determine; it depends upon the location of the ^{153}Gd marker within the LV, distance of the marker from the endocardial surface, and the cardiac dynamics of each dog. In this study, some ^{153}Gd sources were found as far as 1 cm away from the endocardial surface of the LV. With ED bias distances this large, it would be expected that systolic wall thickening would cause the ES bias distance to be larger than the bias distance used in the error measurement. This additional distance would be subtracted from the stated errors at ES, so that any positive error would decrease, and any negative error would increase.

The correlations of experimental and thermodilution stroke volumes were encouraging. Although it is impossible to determine how much error is involved, thermodilution measurements are subject to several potential sources of error. Errors in the stroke volumes determined experimentally from TRVG most likely were due to errors in ES volume calculations, since the ES images were usually of poorer quality due to the extremely small LV volumes of canine hearts at end-systole.

The patient studies did not quantitatively validate the processing methods described here. ED and ES volumes measured from contrast ventriculograms require several geometric assumptions regarding ventricular shape and are not an ideal "gold standard" for comparison. Comparisons of known coronary artery stenoses with regions of reduced wall motion were

qualitative. Nevertheless, the areas of reduced wall motion corresponded well with the distribution of high grade coronary artery stenoses (Fig. 8). Thus, the potential for the clinical use of this technique appears favorable.

CONCLUSION

These studies have demonstrated that it is possible to quantify regional wall motion in three-dimensional from tomographic radionuclide ventriculograms. Specifically, it was shown that the three-dimensional processing methods described here can accurately identify the LV surface prefatory to the calculation of local, regional, and global ventricular motion, area, and volume. We conclude that these techniques for the quantification and display of LV wall motion demonstrate excellent potential and should be highly reliable and useful in clinical use.

REFERENCES

1. Rigo P, Murray M, Strauss HW, et al. Left ventricular function in acute myocardial infarction evaluated by gated scintiphotography. *Circulation* 1974; 50:678–684.
2. Marshall RC, Berger HJ, Costin JC, et al. Assessment of cardiac performance with quantitative radionuclide angiocardiography. Sequential left ventricular ejection fraction, normalized left ventricular ejection fraction, and regional wall motion. *Circulation* 1977; 56:820–829.
3. Jengo JA, Mena I, Blaufuss A, et al. Evaluation of left ventricular function (ejection fraction and segmental wall motion) by single pass radioisotope angiography. *Circulation* 1978; 57:326–332.
4. Maddox DE, Holman BL, Wynne J, et al. Ejection fraction image: a non-invasive index of regional left ventricular wall motion. *Am J Cardiol* 1978; 41:1230–1238.
5. Slack JD, Landon JK, Cole JS. Biplane regional wall motion analysis: optimal method for identification of left ventricular akineses/dyskineses with quantitative cineangiography in man. *Comput Med Biol* 1981; 11:21–32.
6. Vos PH, Vossepoel AM, Pauwels EKJ. Quantitative assessment of wall motion in multiple gated studies using temporal fourier analysis. *J Nucl Med* 1983; 24:388–396.
7. Vitale DF, Green MV, Bacharach SL, et al. Assessment of regional left ventricular function by sector analysis: a method for objective evaluation of radionuclide blood pool studies. *Am J Cardiol* 1983; 52:1112–1119.
8. Dehmer GJ, Lewis SE, Hillis LD, et al. Nongeometric determination of left ventricular volumes from equilibrium blood pool scans. *Am J Cardiol* 1980; 45:293–300.
9. Strauss HW, Zaret BL, Hurley PJ, et al. A scintiphotographic method for measuring left ventricular ejection fraction in man without cardiac catheterization. *Am J Cardiol* 1971; 28:575–580.
10. Schelbert HR, Verba JW, Johnson AD, et al. Noninvasive determination of left ventricular ejection fraction by radionuclide angiography. *Circulation* 1975; 51:902–909.
11. Greene DG, Carlisle R, Grant C, et al. Estimation of left ventricular volume by one-plane cineangiography. *Circulation* 1967; 35:61–69.
12. Sandler H, Dodge H. The use of single plane angiocardiograms for the calculation of left ventricular volume in man. *Am Heart J* 1968; 73:325–334.
13. Kennedy JW, Trenholme SE, Kasser IS. Left ventricular volume and mass from single plane cineangiograms. A comparison of anteroposterior and right anterior oblique methods. *Am Heart J* 1970; 80:344–352.
14. Graham MM, Caputo GR. Measurement of left ventricular volume using emission computed tomography. In: Esser PD, ed. *Emission Computed Tomography.* New York: Society of Nuclear Medicine, 1983:147–153.
15. Gill JB, Moore RH, Tamaki N, Miller DD, Barlai-Kovach M, Yasuda T, Boucher CA, Strauss HW. Multigated blood-pool tomography: new method for the assessment of left ventricular function. *J Nucl Med* 1986; 27:1916–1924.
16. Corbett JR, Jansen DE, Lewis SE, et al. Tomographic gated blood pool radionuclide ventriculography: an analysis of wall motion and left ventricular volumes in patients with coronary artery disease. *J Am College Cardiol* 1985; 6:349–358.
17. Barat J-L, Brendel J, Colle J-P, et al. Quantitative analysis of left ventricular function using gated single photon emission tomography. *J Nucl Med* 1984; 25:1167–1174.
18. Tamaki N, Mukai T, Ishii Y, et al. Multiaxial tomography of heart chambers by gated blood pool emission computed tomography using a rotating gamma camera. *Radiology* 1983; 147:547–554.
19. Duncan JS. Intelligent determination of left ventricular wall motion from multiple view, nuclear medicine image sequences. *Proceedings of the IEEE Computer Society International Symposium on Medical Images and Icons.* 1984:265–269.
20. Bunke H, Feistl H, Neimann H, et al. Smoothing, thresholding, and contour extraction in images from gated blood pool studies. Proc 1st IEEE Computer Society International Symposium on Medical Imaging and Image Interpretation. 1982:146–151.
21. Lie SP, Reiber JHC, Hoek C, et al. Automated boundary extraction from cardiac scintigrams. *Proceedings of the 7th International Meeting on Information Processing in Medical Imaging.* 1981:310–328.
22. Harris LD, Clayton PD, Marshall HW, et al. A Technique for the Detection of Asynergistic Motion in The Left Ventricle, *Comput Biomed Res* 1974; 7:380–394.
23. Ingels NB, Mead CW, Daughters GT, et al. A new model for assessment of left ventricular wall motion. *Proc IEEE Comput Cardiol* 1978; 57–61.
24. Alderman EL, Schwartzkopf A, Ingels NB, et al. An application of an externally referenced polar coordinate system for left ventricular wall motion analysis. *Proc IEEE Comput Cardiol* 1979; 207–210.
25. Bjelogrlic Z, Jakopin J, Gyergyek L. Clustering of Left Ventricular Wall Motion Patterns. *Proceedings of the 1st IEEE Computer Society International Symposium on Medical Imaging and Image Interpretation.* 1982; 117–122.
26. Leighton RF, Wilt SM, Lewis RP. Detection of hy-

pokinesis by a quantitative analysis of left ventricular cineangiograms. *Circulation* 1974; 50:121–127.
27. Bolson EL, Kliman S, Sheehan F, et al. Left ventricular segmental wall motion—a new method using local direction information. *Proc IEEE Comput Cardiol* 1980; 245–248.
28. Doss JK, Hillis LD, Curry G, et al. A new model for the assessment of regional ventricular wall motion. *Radiology* 1982; 143:763–770.
29. Slager CJ, Hooghoudt TEH, Serruys PW, et al. Quantitative assessment of regional left ventricular motion using endocardial landmarks. *J Am Coll Cardiol* 1986; 7:2, 317–326.
30. Ingels NB, Daughters GT, Stinson EB, et al. Evaluation of methods of quantitating left ventricular segmental wall motion in man using myocardial markers as a standard. *Circulation* 1980; 61:966–972.
31. Neumann P, Shicha H, Tebbe U, et al. Analysis of left ventricular regional motility: a comparison of different methods. *Eur J Nucl Med* 1984; 9:205–208.
32. Daughters GT, Schwarzkopf A, Mead CW, et al. A clinical evaluation of five techniques for left ventricular wall motion assessment. *Proc IEEE Comput Cardiol* 1980; 249–252.
33. Mitchell JH, Wildenthal K, Mullins CB. Geometrical studies of the left ventricle utilitizing biplane cinefluorography. *Fed Proc* 1969; 28:1334–1343.
34. Ingels NB, Daughters GT, Stinson EB, et al. Measurement of midwall myocardial dynamics in intact man by radiography of surgically implanted markers. *Circulation* 1975; 52:859–867.
35. Smith TD, Richards P. A simple kit for the preparation of Tc-99m-labelled red blood cells. *J Nucl Med* 1976; 17:126–132.
36. Faber TL, Stokely EM. Feature detection in 3-d medical images using shape information. *IEEE Trans Med Imag* 1987; MI-6(1):8–13.
37. Newman WM, Sproull RF. Principles of Interactive Computer Graphics. 2nd ed. New York: McGraw-Hill, 1979.
38. Chow CK, Kaneko T. Automatic boundary detection of the left ventricle from cineangiograms. *Comput Biomed Res* 1972; 5:388–410.
39. Tauxe WN, Soussaline F, Todd-Pokropek A, et al. Determination of Organ Volume by Single Photon Emission Tomography. *J Nucl Med* 1982; 23:984–987.
40. Tamaki N, Mukai T, Ishii Y, et al. Comparative study of thallium emission myocardial tomograph with 180° and 360° data collection. *J Nucl Med* 1982; 23:661–666.
41. Bacharach SL, Green MV, Borer JS, et al. Left ventricular peak ejection rate, filling rate, and ejection fraction—frame rate requirements at rest and exercise: concise communication. *J Nucl Med* 1979; 20:189–193.